IOP Publishing Modelling and Simulation in Materials Science and Engineering
Modelling Simul. Mater. Sci. Eng. **30** (2022) 024004 (18pp) https://doi.org/10.1088/1361-651X/ac466c

Energy quadratization Runge–Kutta method for the modified phase field crystal equation

Jaemin Shin[1], Hyun Geun Lee[2] and June-Yub Lee[3,*]

[1] Department of Mathematics, Chungbuk National University, Cheongju 28644, Republic of Korea
[2] Department of Mathematics, Kwangwoon University, Seoul 01897, Republic of Korea
[3] Department of Mathematics, Ewha Womans University, Seoul 03760, Republic of Korea

E-mail: jyllee@ewha.ac.kr

Received 3 October 2021, revised 16 December 2021
Accepted for publication 25 December 2021
Published 11 January 2022

Abstract

In this paper, we propose high order and unconditionally energy stable methods for a modified phase field crystal equation by applying the strategy of the energy quadratization Runge–Kutta methods. We transform the original model into an equivalent system with auxiliary variables and quadratic free energy. The modified system preserves the laws of mass conservation and energy dissipation with the associated energy functional. We present rigorous proofs of the mass conservation and energy dissipation properties of the proposed numerical methods and present numerical experiments conducted to demonstrate their accuracy and energy stability. Finally, we compare long-term simulations using an indicator function to characterize the pattern formation.

Keywords: modified phase field crystal equation, energy quadratization Runge–Kutta method, unconditional energy stability, mass conservation

(Some figures may appear in colour only in the online journal)

1. Introduction

We consider an energy quadratization Runge–Kutta (EQRK) method for constructing unconditionally energy stable schemes used in a modified phase field crystal (MPFC) equation [1, 2]

*Author to whom any correspondence should be addressed.

$$\frac{\partial^2\phi}{\partial t^2} + \beta\frac{\partial\phi}{\partial t} = M\Delta\left(F'(\phi) + (1+\Delta)^2\phi\right), \tag{1}$$

where ϕ is the atomic density field, β is a positive constant, and $M > 0$ is a mobility constant. We consider a typical polynomial

$$F(\phi) = \frac{1}{4}\phi^4 - \frac{\epsilon}{2}\phi^2, \tag{2}$$

where ϵ is a positive constant with physical significance. This system can be completed by assuming that ϕ is periodic on a domain Ω in $\mathbb{R}^d$ $(d = 1, 2, 3)$.

In this study, we develop a numerical method such that two physical structures (i.e. mass conservation and energy dissipation) are preserved. If the initial condition satisfies $\int_\Omega \frac{\partial\phi}{\partial t}(\mathbf{x}, 0)\,\mathrm{d}\mathbf{x} = 0$, then the mass is conserved over time; that is,

$$\frac{\mathrm{d}}{\mathrm{d}t}\int_\Omega \phi(\mathbf{x}, t)\,\mathrm{d}\mathbf{x} = 0. \tag{3}$$

In addition, the solutions to (1) dissipate the following energy.

$$\mathcal{F}(\phi) = \langle F(\phi), 1\rangle + \frac{1}{2}\left\langle \phi, (1+\Delta)^2\phi\right\rangle + \frac{1}{2M}\left\|\frac{\partial\phi}{\partial t}\right\|^2_{H^{-1}}, \tag{4}$$

where $\langle f, g\rangle$ and $\langle f, g\rangle_{H^{-1}}$ are the L^2- and H^{-1}-inner products, respectively. Possessing an energy decreasing property at the discrete level implies that the scheme is energy stable. In addition, an unconditionally energy stable scheme does not have any restrictions on the time step size.

From a physical perspective, the phase field crystal (PFC) equation

$$\frac{\partial\phi}{\partial t} = M\Delta\left(F'(\phi) + (1+\Delta)^2\phi\right), \tag{5}$$

has been proposed to model atomic-scale elastic interactions as well as crystal plasticity and diffusive dynamics [3, 4]. The PFC equation (5) successfully simulates the dynamics of polycrystalline grain boundaries, grain-boundary energy, and dislocation. However, distinguishing the elastic relaxation and diffusive time scales is difficult. Meanwhile, the MPFC equation (1) was introduced to simulate rapid elastic relaxation over long length scales by introducing the second-order time derivatives [1, 2]. From a mathematical perspective, the PFC equation is described by a gradient flow for the Swift–Hohenberg energy functional

$$\mathcal{F}_{\mathrm{PFC}}(\phi) = \langle F(\phi), 1\rangle + \frac{1}{2}\left\langle \phi, (1+\Delta)^2\phi\right\rangle, \tag{6}$$

under the H^{-1} inner product space. Because the PFC equation is of a gradient type, it may be straightforwardly noted that the energy (6) does not increase over time. Meanwhile, the MPFC model is no longer a gradient flow. However, the original energy (6) with a kinetic energy term becomes pseudo-energy (4), which does not increase over time.

Owing to the wide coverage of a gradient flow for the phase field model, many unconditionally energy stable schemes have been developed with high accuracy. For examples, see [5–11] and therein. Specifically, using the PFC equation, many works on convex splitting

methods [5, 12–14], secant-type difference [15], a modified Crank–Nicolson method [16], and energy quadratization (EQ) strategies [9, 10, 17] have been reported in the relevant literature. Despite the difference between the damped wave equation (1) and diffusive equation (5), the similarity of the equations and their properties have attracted many researchers to focus on numerical methods for extending the PFC equation to the MPFC equation, including convex splitting methods [18, 19], secant-type difference [20], a modified Crank–Nicolson method [21], and EQ strategies [22–24].

Among the presented studies, the convex splitting Runge–Kutta (CSRK) method [14] was recently proposed to solve the PFC equation with high order time accuracy and unconditional energy stability. However, the applicability of the CSRK scheme to the MPFC equation remain an open question because it is not a gradient flow. Only a second-order convex splitting method with a backward difference formula has been provided for the MPFC equation [13], which guarantees only the boundedness of its energy functional, and not its dissipative property. In constrast, the EQRK method [10] is a successful framework for the development of unconditionally energy stable schemes. Because the EQRK method is based on the EQ strategy, the method can be applied to various systems even for a non-gradient flow. The aim of the present work is to demonstrate the extendability of the high order EQRK method to the MPFC equation. Because the MPFC equation often requires long-term dynamic simulations to reach a steady state, high order accurate energy stable schemes are desirable to render large step sizes practical while preserving accuracy compared to existing second-order methods.

The remainder of this paper is organized as follows. Section 2 describes a detailed reformulation using EQ, a derivation of the EQRK method, and issues related to the numerical implementation. Section 3 presents numerical results showing the accuracy and energy stability of the proposed method. Finally, some concluding remarks are provided in section 4.

2. Numerical scheme

We first introduce a reformulated system with EQ by defining an auxiliary variable. Next, we apply the EQRK concept to the reformulation. With a well-known algebraic stability condition for the coefficients of RK methods, we provide some proofs of the energy stability and mass conservation of the proposed approach. Finally, for the numerical test, we present a detailed implementation by choosing the RK class, called the singly diagonally implicit Runge–Kutta method.

2.1. EQ reformulation

We utilize the invariant energy quadratization (IEQ) approach by introducing an auxiliary variable

$$q(\mathbf{x}, t) = \sqrt{F(\phi) + C_0}, \tag{7}$$

where C_0 is a positive constant such that $F(\phi) + C_0 > 0$. For the Swift–Hohenberg models, $F(\phi)$ often has a lower bound; thus, we can choose a proper constant for C_0. In this study, $C_0 = \frac{1}{2}\epsilon^2$ is a suitable choice for a typical example (2). We can then rewrite the original equation (1) as the IEQ reformulated system

$$\begin{aligned}
\frac{\partial \phi}{\partial t} &= \psi, \\
\frac{\partial \psi}{\partial t} &= M\Delta\left(G(\phi)\, q + (1+\Delta)^2\phi\right) - \beta\psi, \\
\frac{\partial q}{\partial t} &= \frac{1}{2} G(\phi)\, \psi,
\end{aligned} \tag{8}$$

where

$$G(\phi) = \frac{F'(\phi)}{\sqrt{F(\phi) + C_0}}. \tag{9}$$

This system is completed with the proper initial conditions and periodic boundary conditions for ϕ, ψ, and q. For given initial states of $\phi(\mathbf{x}, 0)$ and $\psi(\mathbf{x}, 0) = \phi_t(\mathbf{x}, 0)$, it is consistently defined as $q(\mathbf{x}, 0) = \sqrt{F(\phi(\mathbf{x}, 0)) + C_0}$. Furthermore, $\int_\Omega \psi(\mathbf{x}, 0)\mathrm{d}\mathbf{x} = 0$ should be satisfied. The energy functional (4) can be rewritten as a quadratic form

$$\mathcal{F}_{\mathrm{EQ}}(\phi, \psi, q) = \|q\|^2 + \frac{1}{2}\left\langle \phi, (1+\Delta)^2\phi \right\rangle + \frac{1}{2M}\|\psi\|^2_{H^{-1}}. \tag{10}$$

Moreover, the reformulation conserves the properties of mass conservation and energy dissipation. Integrating (8) over Ω with the periodic boundary condition and letting $\Psi(t) = \int_\Omega \psi \mathrm{d}\mathbf{x}$, we obtain

$$\frac{\mathrm{d}\Psi(t)}{\mathrm{d}t} + \beta\Psi(t) = M\int_{\partial\Omega} \nabla\tilde{\mu}\cdot\mathbf{n}\,\mathrm{d}s - M\int_\Omega \nabla\tilde{\mu}\cdot\nabla 1\,\mathrm{d}\mathbf{x} = 0, \tag{11}$$

where $\tilde{\mu} = G(\phi)\, q + (1+\Delta)^2\phi$ and $\mathbf{n}$ is the unit normal vector to $\partial\Omega$. $\Psi(t) = \Psi(0)e^{-\beta t}$ and $\Psi(0) = 0$ are solutions to the simple ODE (11), which imply mass conservation. In addition, through a straightforward calculation, (8) possesses the following energy dissipation.

$$\begin{aligned}
\frac{\mathrm{d}\mathcal{F}_{\mathrm{EQ}}}{\mathrm{d}t} &= \left\langle q, 2\frac{\partial q}{\partial t}\right\rangle + \left\langle (1+\Delta)^2\phi, \frac{\partial\phi}{\partial t}\right\rangle + \frac{1}{M}\left\langle \psi, \frac{\partial\psi}{\partial t}\right\rangle_{H^{-1}} \\
&= \left\langle q, G(\phi)\,\psi\right\rangle + \left\langle (1+\Delta)^2\phi, \psi\right\rangle + \frac{1}{M}\left\langle \psi, \frac{\partial\psi}{\partial t}\right\rangle_{H^{-1}} \\
&= \frac{1}{M}\left\langle \psi, \frac{\partial\psi}{\partial t} - M\Delta\left(G(\phi)\, q + (1+\Delta)^2\phi\right)\right\rangle_{H^{-1}} \\
&= -\frac{\beta}{M}\|\psi\|^2_{H^{-1}} \leqslant 0.
\end{aligned} \tag{12}$$

2.2. EQRK method

For the RK coefficients $\mathbf{A} \in \mathbb{R}^{s\times s}$, $\mathbf{b} \in \mathbb{R}^s$, and $\mathbf{c} = \mathbf{A1}$, we can construct the following RK method. For given (ϕ^n, ψ^n, q^n), the ith stage intermediate values are calculated by

$$\begin{aligned}\phi_i &= \phi^n + \Delta t\sum_{j=1}^{s} a_{ij}h_j,\\ \psi_i &= \psi^n + \Delta t\sum_{j=1}^{s} a_{ij}k_j,\\ q_i &= q^n + \Delta t\sum_{j=1}^{s} a_{ij}l_j,\end{aligned} \tag{13}$$

where $h_i = \psi_i$, $k_i = M\Delta\left(G(\phi_i)\,q_i + (1+\Delta)^2\phi_i\right) - \beta\psi_i$, and $l_i = \frac{1}{2}G(\phi_i)\,\psi_i$. Then, we evaluate the approximation of the subsequent time step $\left(\phi^{n+1}, \psi^{n+1}, q^{n+1}\right)$ as

$$\begin{aligned}\phi^{n+1} &= \phi^n + \Delta t\sum_{i=1}^{s} b_ih_i,\\ \psi^{n+1} &= \psi^n + \Delta t\sum_{i=1}^{s} b_ik_i,\\ q^{n+1} &= q^n + \Delta t\sum_{i=1}^{s} b_il_i.\end{aligned} \tag{14}$$

We now refer to (14) as IEQ-RK. Before introducing the conditions and proofs, we note that the scalar auxiliary variable (SAV) approach of choosing an auxiliary variable as $q = \sqrt{\langle F(\phi), 1\rangle + C_0}$ is another method of EQ reformulation. We can then consider the combination of SAV and EQRK, which is a straightforward construction. In this paper, we present the EQRK method using only the IEQ formulation.

For an RK table $(\mathbf{A}, \mathbf{b}, \mathbf{c})$ and the corresponding symmetric matrix

$$\mathbf{M} = \mathbf{BA} + \mathbf{A}^{\mathrm{T}}\mathbf{B} - \mathbf{b}\mathbf{b}^{\mathrm{T}}, \tag{15}$$

where $\mathbf{B} = \mathrm{diag}(\mathbf{b})$, we state that an RK method satisfies the *algebraic stability* condition if the matrix $\mathbf{M}$ is positive semi-definite and all components of $\mathbf{b}$ are non-negative.

For a simple description, we define the discrete energy at time t^n as

$$\mathcal{F}_{\mathrm{EQ}}^n = \mathcal{F}_{\mathrm{EQ}}\left(\phi^n, \psi^n, q^n\right). \tag{16}$$

Theorem 1. *The IEQ-RK scheme* (14) *satisfying the algebraic stability condition is unconditionally energy stable; that is,* $\mathcal{F}_{EQ}^{n+1} \leqslant \mathcal{F}_{EQ}^n$.

Proof. Using the equalities for q^{n+1} and q_i, we obtain

$$\begin{aligned}\left\|q^{n+1}\right\|^2 - \left\|q^n\right\|^2 &= 2\Delta t\sum_{i=1}^{s} b_i\left\langle l_i, q^n\right\rangle + \Delta t^2\sum_{i=1}^{s}\sum_{j=1}^{s} b_ib_j\left\langle l_i, l_j\right\rangle\\ &= 2\Delta t\sum_{i=1}^{s} b_i\left\langle l_i, q_i\right\rangle - \Delta t^2\sum_{i=1}^{s}\sum_{j=1}^{s} m_{ij}\left\langle l_i, l_j\right\rangle.\end{aligned} \tag{17}$$

Because of the positive semi-definiteness of **M**, we obtain

$$\left\|q^{n+1}\right\|^2 - \|q^n\|^2 \leqslant 2\Delta t \sum_{i=1}^{s} b_i \langle l_i, q_i\rangle . \tag{18}$$

Similarly, we have

$$\frac{1}{2}\left\langle \phi^{n+1}, (1+\Delta)^2\phi^{n+1}\right\rangle - \frac{1}{2}\left\langle \phi^{n}, (1+\Delta)^2\phi^{n}\right\rangle \leqslant \Delta t \sum_{i=1}^{s} b_i \left\langle h_i, (1+\Delta)^2\phi_i\right\rangle , \tag{19}$$

and

$$\frac{1}{2M}\left\|\psi^{n+1}\right\|_{H^{-1}}^2 - \frac{1}{2M}\|\psi^{n}\|_{H^{-1}}^2 \leqslant \frac{\Delta t}{M}\sum_{i=1}^{s} b_i \langle k_i, \psi_i\rangle_{H^{-1}}. \tag{20}$$

Adding (18), (19), and (20) leads to

$$\mathcal{F}_{\mathrm{EQ}}^{n+1} - \mathcal{F}_{\mathrm{EQ}}^{n} \leqslant \Delta t \sum_{i=1}^{s} b_i \left[2\langle l_i, q_i\rangle + \left\langle h_i, (1+\Delta)^2\phi_i\right\rangle + \frac{1}{M}\langle k_i, \psi_i\rangle_{H^{-1}}\right]. \tag{21}$$

The summand can be extended as

$$\begin{aligned} &2\langle l_i, q_i\rangle + \left\langle h_i, (1+\Delta)^2\phi_i\right\rangle + \frac{1}{M}\langle k_i, \psi_i\rangle_{H^{-1}} \\ &\quad = \langle G(\phi_i)\,\psi_i, q_i\rangle + \left\langle \psi_i, (1+\Delta)^2\phi_i\right\rangle + \frac{1}{M}\langle \psi_i, k_i\rangle_{H^{-1}} \\ &\quad = \frac{1}{M}\left\langle \psi_i, k_i - M\Delta\left(G(\phi_i)\,q_i + (1+\Delta)^2\phi_i\right)\right\rangle_{H^{-1}} = -\frac{\beta}{M}\|\psi_i\|_{H^{-1}}^2. \end{aligned} \tag{22}$$

Finally, (21) can be rewritten as

$$\mathcal{F}_{\mathrm{EQ}}^{n+1} - \mathcal{F}_{\mathrm{EQ}}^{n} \leqslant -\Delta t \frac{\beta}{M}\sum_{i=1}^{s} b_i \|\psi_i\|_{H^{-1}}^2. \tag{23}$$

Because b_i is non-negative for all i, $\mathcal{F}_{\mathrm{EQ}}^{n+1} \leqslant \mathcal{F}_{\mathrm{EQ}}^{n}$ for any time step $\Delta t > 0$. Therefore, the scheme inherits the numerical energy dissipation. □

Theorem 2. *The IEQ-RK scheme* (14) *with* $\langle \psi^n, 1\rangle = 0$ *satisfies* $\left\langle \psi^{n+1}, 1\right\rangle = 0$ *and* $\left\langle \phi^{n+1}, 1\right\rangle = \langle \phi^n, 1\rangle$ *if* $\mathbf{b} \in \mathrm{Null}^{\perp}(I + \beta\Delta t\mathbf{A})$, *that is, the matrix* $I + \beta\Delta t\mathbf{A}$ *is invertible or* **b** *is perpendicular to the null space of* $I + \beta\Delta t\mathbf{A}$.

Proof. Suppose that the method (14) has a solution. From the periodic boundary condition, for any i, we have

$$\langle k_i, 1\rangle = \left\langle M\Delta\left(G(\phi_i)\,q_i + (1+\Delta)^2\phi_i\right) - \beta\psi_i, 1\right\rangle = -\beta\langle \psi_i, 1\rangle . \tag{24}$$

For each stage, taking an inner product with 1, we have

$$\langle \psi_i, 1\rangle = \langle \psi^n, 1\rangle + \Delta t \sum_{j=1}^{s} a_{ij} \langle k_j, 1\rangle = -\beta \Delta t \sum_{j=1}^{s} a_{ij} \langle \psi_j, 1\rangle . \tag{25}$$

If $I + \beta\Delta t\mathbf{A}$ is invertible, then $\langle \psi_i, 1\rangle = 0$ for all i. Otherwise, $\mathbf{b}$ is perpendicular to any solution of the homogeneous matrix equation $\sum_{i=1}^{s} b_i \langle \psi_i, 1\rangle = 0$. Then, we have

$$\left\langle \psi^{n+1}, 1\right\rangle = \langle \psi^n, 1\rangle + \Delta t \sum_{i=1}^{s} b_i \langle k_i, 1\rangle = 0, \tag{26}$$

and

$$\left\langle \phi^{n+1}, 1\right\rangle = \langle \phi^n, 1\rangle + \Delta t \sum_{i=1}^{s} b_i \langle h_i, 1\rangle = \langle \phi^n, 1\rangle . \tag{27}$$

□

Corollary 3. *Suppose that* $\left\langle \psi^0, 1\right\rangle = 0$. *Then, the IEQ-RK scheme* (14) *satisfying the algebraic stability condition is mass-conserving; that is,* $\langle \phi^n, 1\rangle = \left\langle \phi^0, 1\right\rangle$.

Proof. With the initial state of $\left\langle \psi^0, 1\right\rangle = 0$, we can easily show that $\langle \psi^n, 1\rangle = 0$ and $\langle \phi^n, 1\rangle = \left\langle \phi^0, 1\right\rangle$ for all $n \geqslant 1$, based on mathematical induction. We need only prove the condition $\mathbf{b} \in \text{Null}^{\perp}(I + \beta\Delta t\mathbf{A})$ using the algebraic stability condition; that is, $\mathbf{M}$ is positive semi-definite and $\mathbf{B} = \text{diag}\,(\mathbf{b})$ is non-negative. If the matrix of $I + \beta\Delta t\mathbf{A}$ is invertible, then the condition holds. Suppose the matrix is not invertible; then, there exists a nonzero vector χ such that $\chi + \beta\Delta t\mathbf{A}\chi = 0$ or $\mathbf{A}\chi = \frac{-1}{\beta\Delta t}\chi$. Based on the definition of $\mathbf{M}$ in (15),

$$\begin{aligned}(\chi, \mathbf{M}\boldsymbol{\chi}) &= (\chi, \mathbf{BA}\chi) + (\chi, \mathbf{A}^{\mathrm{T}}\mathbf{B}\chi) - (\chi, \mathbf{b}\mathbf{b}^{\mathrm{T}}\chi) \\ &= 2(\mathbf{B}\chi, \mathbf{A}\chi) - (\mathbf{b}^{\mathrm{T}}\chi)^2 = \frac{-2}{\beta\Delta t}(\mathbf{B}\chi, \chi) - (\mathbf{b}^{\mathrm{T}}\chi)^2 \leqslant 0.\end{aligned} \tag{28}$$

Using the positive semi-definiteness of $\mathbf{M}$ and positivity of $\mathbf{B}$, we conclude that $(\chi, \mathbf{M}\chi) = 0$ and $\mathbf{b}^{\mathrm{T}}\chi = 0$, which implies $\mathbf{b} \in \text{Null}^{\perp}(I + \beta\Delta t\mathbf{A})$. □

2.3. Diagonally implicit Runge–Kutta methods

Diagonally implicit Runge–Kutta methods can be a reasonable choice to circumvent the difficulty of solving the full system. The Butcher notation indicates that $\mathbf{A}$ is a lower triangular matrix. For self-consistency, we present examples of the singly diagonally implicit Runge–Kutta (SDIRK) tables [10] in table 1 satisfying the algebraic stability condition (positive semi-definite $\mathbf{M}$ in (15) and non-negative $\mathbf{b}$). Please refer to [25, 26] for further discussion. For the numerical test, we refer to as EQRK(p) for the desired pth order of accuracy.

In this section, we present the detailed implementation of (13) with the SDIRK methods in table 1. For each ith stage, we need to solve the nonlinear system

Table 1. Butcher tableaus of SDIRK, where $\lambda = \left(3+\sqrt{3}\right)/6$, $\sigma = \cos\left(\frac{\pi}{18}\right)/\sqrt{3} + 1/2$, and $\mu = 1/\left(6(2\sigma-1)^2\right)$.

EQRK(1)

1	1
	1

EQRK(2)

$\frac{1}{2}$	$\frac{1}{2}$
	1

EQRK(3)

λ	λ	0	
$1-\lambda$	$1-2\lambda$	λ	
	$\frac{1}{2}$	$\frac{1}{2}$	

EQRK(4)

σ	σ	0	0
$\frac{1}{2}$	$\frac{1}{2}-\sigma$	σ	0
$1-\sigma$	2σ	$1-4\sigma$	σ
	μ	$1-2\mu$	μ

$$\begin{aligned} \phi_i - a_{ii}\Delta t\psi_i &= S_i^h, \\ \left(1+\beta a_{ii}\Delta t\right)\psi_i - Ma_{ii}\Delta t\Delta\left(G\left(\phi_i\right)q_i + (1+\Delta)^2\phi_i\right) &= S_i^k, \\ q_i - \frac{1}{2}a_{ii}\Delta tG\left(\phi_i\right)\psi_i &= S_i^l, \end{aligned} \tag{29}$$

where $S_i^h = \phi^n + \Delta t\sum_{j=1}^{i-1} a_{ij}h_j$, $S_i^k = \psi^n + \Delta t\sum_{j=1}^{i-1} a_{ij}k_j$, and $S_i^l = q^n + \Delta t\sum_{j=1}^{i-1} a_{ij}l_j$. We can simply represent this nonlinear system (29) as

$$\mathcal{N}\left(\phi_i, \psi_i, q_i\right) = \left(S_i^h, S_i^k, S_i^l\right). \tag{30}$$

To construct the nonlinear iterative method for (29), we apply Newton's method and recursively solve the following linear system.

$$\nabla\mathcal{N}^m \begin{bmatrix} \phi_i^{m+1} - \phi_i^m \\ \psi_i^{m+1} - \psi_i^m \\ q_i^{m+1} - q_i^m \end{bmatrix} = \begin{bmatrix} S_i^{h,m} \\ S_i^{k,m} \\ S_i^{l,m} \end{bmatrix}, \tag{31}$$

where

$$\nabla\mathcal{N}^m = \begin{bmatrix} I & -a_{ii}\Delta t & 0 \\ -Ma_{ii}\Delta t\Delta\left(G'\left(\phi_i^m\right)q_i^m + (I+\Delta)^2\right) & I + \beta a_{ii}\Delta t & -Ma_{ii}\Delta t\Delta G\left(\phi_i^m\right) \\ -\frac{1}{2}a_{ii}\Delta tG'\left(\phi_i^m\right)\psi_i^m & -\frac{1}{2}a_{ii}\Delta tG\left(\phi_i^m\right) & I \end{bmatrix}, \tag{32}$$

$$\left(S_i^{h,m}, S_i^{k,m}, S_i^{l,m}\right) = \left(S_i^h, S_i^k, S_i^l\right) - \mathcal{N}\left(\phi_i^m, \psi_i^m, q_i^m\right). \tag{33}$$

Here, $G'(\phi)$ can be written as

$$G'(\phi) = \frac{2F''(\phi)F(\phi) - \left(F'(\phi)\right)^2 + 2C_0F''(\phi)}{2\left(F(\phi)+C_0\right)^{\frac{3}{2}}}. \tag{34}$$

To execute the iteration, we set the initial state as $\phi_i^0 = \phi_{i-1}$ and obtain the solution to (29) at the ith stage by $\phi_i = \phi_i^{m+1}$ if the relative l_2-norm of the consecutive error $\frac{\left\|\phi_i^{m+1} - \phi_i^m\right\|}{\left\|\phi_i^m\right\|}$ is less than the tolerance tol.

To reduce the computational cost by constructing an inversion algorithm for $\nabla\mathcal{N}^m$, we introduce a reduction strategy. Through an algebraic manipulation, (31) can be reduced only for

ψ_i^{m+1} as

$$\mathcal{L}^m \left(\psi_i^{m+1} - \psi_i^m\right) = S^m, \tag{35}$$

where

$$\mathcal{L}^m = I + \beta a_{ii}\Delta t - (a_{ii}\Delta t)^2 M\Delta \left(\eta^m + (I+\Delta)^2\right), \tag{36}$$

$$\eta^m = G'\left(\phi_i^m\right) q_i^m + \frac{1}{2} a_{ii}\Delta t G\left(\phi_i^m\right) G'\left(\phi_i^m\right) \psi_i^m + \frac{1}{2} G^2\left(\phi_i^m\right), \tag{37}$$

and

$$\begin{aligned} S^m = S_i^{k,m} + a_{ii}\Delta t\, M\Delta \Bigg(& G'\left(\phi_i^m\right) q_i^m S_i^{h,m} + \frac{1}{2} a_{ii}\Delta t\, G\left(\phi_i^m\right) G'\left(\phi_i^m\right) \psi_i^m S_i^{h,m} \\ & + G\left(\phi_i^m\right) S_i^{l,m} + (1+\Delta)^2 S_i^{h,m} \Bigg). \end{aligned} \tag{38}$$

Next, we calculate ϕ_i^{m+1} and q_i^{m+1} by

$$\begin{aligned} \phi_i^{m+1} &= \phi_i^m + S_i^{h,m} + a_{ii}\Delta t \left(\psi_i^{m+1} - \psi_i^m\right), \\ q_i^{m+1} &= q_i^m + S_i^{l,m} + \frac{1}{2} a_{ii}\Delta t\, G\left(\phi_i^m\right)\left(\psi_i^{m+1} - \psi_i^m\right) + \frac{1}{2} a_{ii}\Delta t\, G'\left(\phi_i^m\right)\psi_i^m\left(\phi_i^{m+1} - \phi_i^m\right). \end{aligned} \tag{39}$$

To solve (35) numerically, we employ the bi-conjugate gradient (BICG) method. In addition, to accelerate the convergence rate of the linear solver for (35), we consider a preconditioner as

$$P = I + \beta a_{ii}\Delta t - (a_{ii}\Delta t)^2 M\Delta(I + \Delta^2). \tag{40}$$

3. Numerical experiments

3.1. Numerical convergence with a smooth initial condition in 1D

We numerically demonstrate the convergence and the unconditional energy stability of the proposed method (14) as well as the numerical solvability of the nonlinear system of equation (29) using the following smooth initial condition,

$$\begin{aligned} \phi(x,0) &= 0.07 - 0.02\cos\left(\frac{2\pi(x-12)}{32}\right) + 0.02\cos^2\left(\frac{\pi(x+10)}{32}\right) - 0.01\sin^2\left(\frac{4\pi x}{32}\right), \\ \psi(x,0) &= 0.1\sin\left(\frac{\pi x}{16}\right) - 0.1\cos\left(\frac{\pi x}{16}\right), \\ q(x,0) &= \sqrt{F(\phi(x,0)) + C_0}, \end{aligned} \tag{41}$$

on the one-dimensional domain $\Omega = [0, 32]$. For the other parameters, we set $M = 1$, $\beta = 1$, $\epsilon = 0.25$, and $T = 128$, and the grid size is fixed to $\Delta x = 1/2$, which provides sufficient

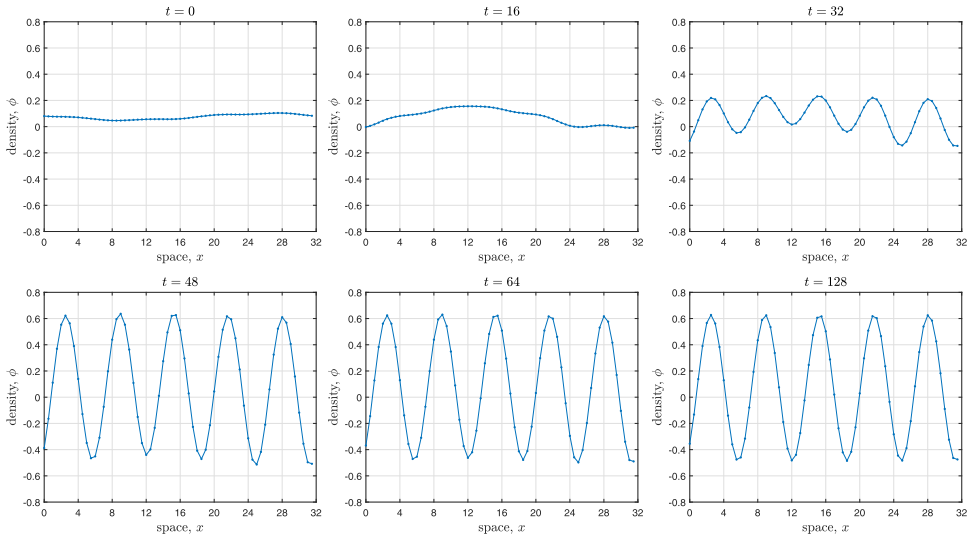

Figure 1. Evolution of the reference solution $\phi(x, t)$.

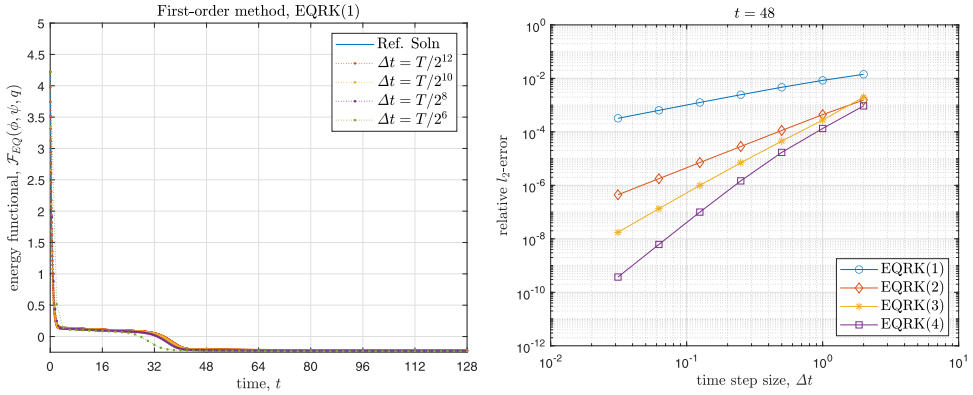

Figure 2. Energy evolution and relative l_2-error with respect to time step sizes Δt.

spatial accuracy. Figure 1 shows the time evolution of the reference solution using the fourth-order method with a sufficiently small time step, $\Delta t = T/2^{14}$. The solution changes to a wave profile at an earlier stage, and the magnitude dramatically increases up to the equilibrium solution.

To verify the energy stability of the proposed approach and estimate its order of convergence with respect to Δt, simulations are conducted by varying $\Delta t = T/2^{12}, T/2^{10}, \ldots, T/2^{6}$. Figure 2 shows the energy evolutions of the first-order method and the relative l_2-errors for the numerical solution with various time steps Δt. We observe the energy dissipation and find that all methods show the desired order of convergence.

The proposed method guarantees the mass conservation regardless of the time step size. Figure 3 shows that the masses computed using the proposed methods maintain the initial constant up to the maximum precision of the machine and inherent rounding errors.

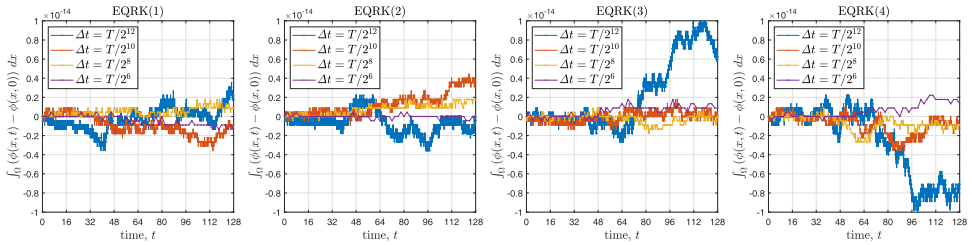

Figure 3. Mass evolution with respect to time step sizes Δt.

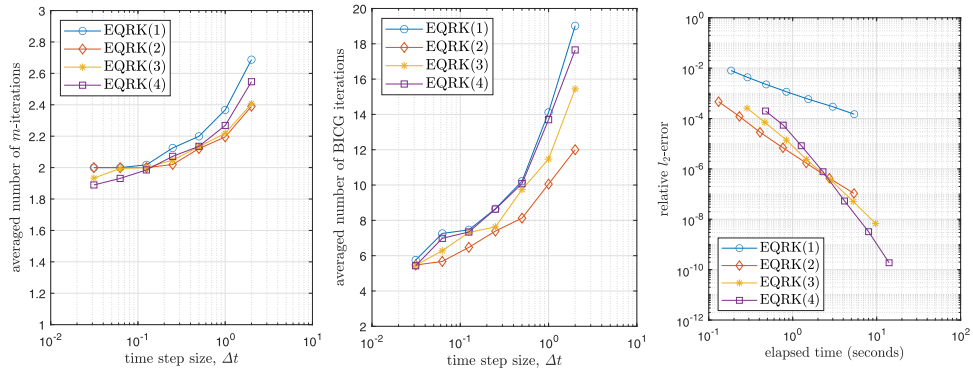

Figure 4. Averaged number of m-iterations and BICG iterations using Newton's method and relative l_2-error with respect to computational time.

We now demonstrate the numerical solvability of the system of nonlinear equation (29) and the computational efficiency of solving (31) and (35). We count the numbers of the nonlinear iteration for (31) and the BICG iteration for (35) by varying $\Delta t = T/2^{12}, T/2^{11}, \ldots, T/2^{6}$. The stopping criterion for the nonlinear iteration is a relative l_2-norm of the consecutive error of less than $\mathrm{tol} = 10^{-6}$ and that for the BICG iteration is the relative residual norm of less than $\mathrm{tol} = 10^{-6}\Delta t$. The leftmost and the middle plots in figure 4 show the average number of nonlinear and BICG iterations for each stage up to $T = 128$. Two or three iterations of the nonlinear solver are involved in proceeding to the next stage. We believe that such a rapid iterative convergence may be possible by using a Newton-type iteration method, and the resulting linear subsystems are numerically well-conditioned even for relatively large time steps. Here, the number of BICG iterations depends on the condition number of the linear operator $\mathcal{L}^m = I + \beta a_{ii}\Delta t + O(\Delta t^2)$ defined in (35). For relatively large Δt, the EQRK(2) with $a_{ii} = 1/2$ is the fastest method, and EQRK(3) with $a_{ii} = \lambda \approx 0.7887$ is slightly faster than EQRK(1) with $a_{ii} = 1$ or EQRK(4) with $a_{ii} = \sigma \approx 1.0686$.

The rightmost plot in figure 4 shows the relative l_2-errors of the numerical solution $\phi(\cdot, t = 128)$ with respect to the elapsed time. The computational time is measured using MATLAB(Ver 2020b) on a machine running the Linux operating system with dual Xeon 4216 CPUs and 128 GB of RAM. The computational cost is proportional to the multiplication of m-iteration, BICG iteration, and the stage numbers $(1, 1, 2, 3$ for EQRK$(p = 1, 2, 3, 4))$. We note that the computational cost EQRK(3 or 4) is about two or three times more expensive than

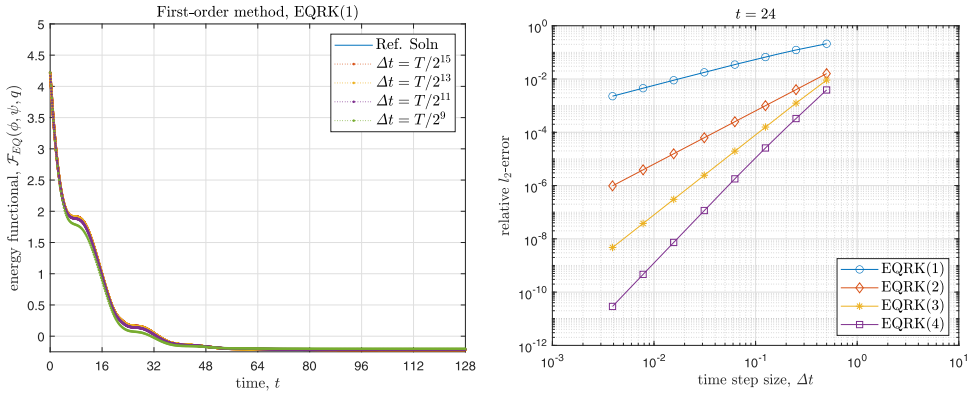

Figure 5. Energy evolution and relative l_2-error for the case of $\beta = 0.1$.

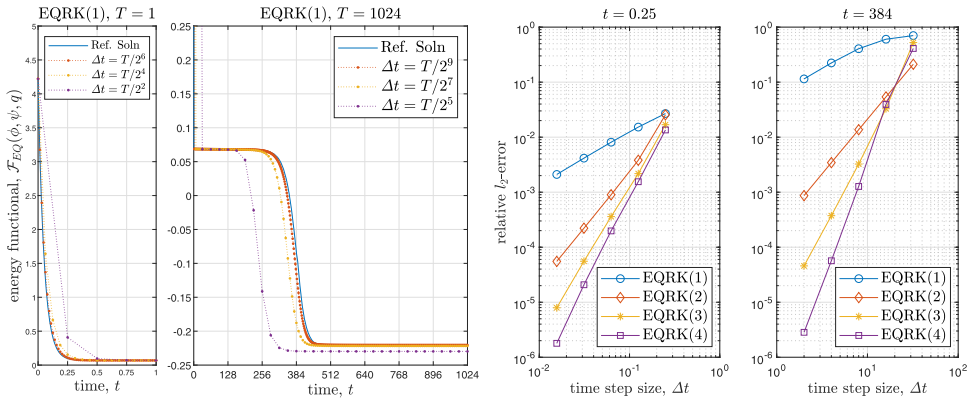

Figure 6. Energy evolution and relative l_2-error for the case of $\beta = 10$.

EQRK(1 or 2) for fixed Δt, but EQRK(3 or 4) exhibites far better performance when relatively high accuracy is preferred.

Next, we present the numerical results for different values of β. Figures 5 and 6 show the energy evolution and the relative l_2-errors of the numerical solutions for $\beta = 0.1$ and $\beta = 10$ given the same initial condition and parameters as those in figure 2. Figure 5 shows the desired order of convergence for $\beta = 0.1$ with $\Delta t = T/2^{15}, T/2^{14}, \ldots, T/2^{8}$ and $T = 128$. For a larger beta with a larger initial momentum, the physical behavior of the system is slightly more complicated because the energy decays initially rapidly owing to the gradient term $\frac{1}{2M}\left\|\frac{\partial\phi}{\partial t}\right\|^2_{H^{-1}}$ and then slowly varies when the solution forms a pattern. Two clearly different time scales are shown in figure 6. Therefore, we choose $\Delta t = T/2^{6}, T/2^{5}, \ldots, T/2^{2}$ for $T = 1$ to capture fast-decaying modes. We then set $\Delta t = T/2^{9}, T/2^{8}, \ldots, T/2^{5}$ for $T = 1024$, and the first bootstrap step is adaptively refined by $\Delta t/64$. We numerically confirm that the desired order of convergence is observed regardless of the value of parameter β.

We remark that the corresponding energy evolutions for the higher-order methods are closer to the reference solution obtained by the fourth-order method with a quadrupled over-resolved numerical solution. In addition, we only provide results for the energy evolution and numerical

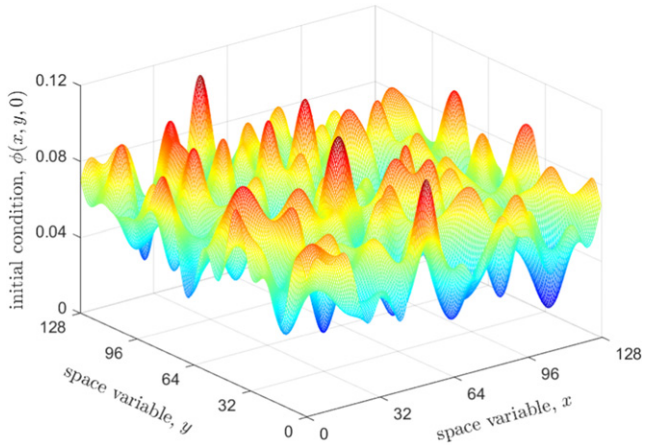

Figure 7. Initial condition profile.

convergence test because the solution profile, mass conservation, and iterative performance are not significantly differ from those for the case of $\beta = 1$.

3.2. Numerical evolution with a randomly perturbed initial condition in 2D

In this section, we employ the fourth-order method to obtain sufficiently accurate results and evolve the MPFC equation with the periodic boundary condition on the two-dimensional domain $\Omega = [0, 128] \times [0, 128]$. For the numerical simulation, we set the randomly perturbed initial condition

$$\begin{aligned} &\phi(x, y, 0) = 0.06 + 0.005 \sum_{l=0}^{8} \sum_{m=0}^{8} \mathrm{Re}\left[a_{lm} e^{\frac{2\pi i l x}{128}}\right] \cdot \mathrm{Re}\left[b_{lm} e^{\frac{2\pi i m y}{128}}\right], \\ &\psi(x, y, 0) = 0, \\ &q(x, y, 0) = \sqrt{F(\phi(x, y, 0)) + C_0}, \end{aligned} \tag{42}$$

where complex numbers $\|a_{lm}\|_\infty \leqslant 1$ and $\|b_{lm}\|_\infty \leqslant 1$ are chosen randomly. However, these values are fixed for the simulations described in this subsection. The smooth initial condition with all 81 possible low-frequency modes is shown in figure 7, where the red, green, and blue regions indicate $\phi = 0.12$, 0.06, and 0.01, respectively.

To show the convergence of the energy evolution for $\beta = 0.1$, 1, and 10, we conduct simulations with various time step sizes Δt. For the computations, we fix the other parameters to $M = 1$, $\epsilon = 0.13$, and $\Delta x = \Delta y = 1/2$. Figure 8 shows the energy evolutions and the relative absolute error over time. We take the quadratically over-resolved numerical solution for each β as the reference solutions. The evolutional time scale slows when the value of β increases; thus, we set the larger final time and temporal step sizes for the larger β. In general, the energy also converges the reference solution when the time step decreases. The height of the cursor shape in the plots represents 16 times in relative errors. For the subsequent 2D simulations, to guarantee three digits of accuracy, we set $\Delta t = 2^{-1}$, 2, and 2^4 for $\beta = 0.1$, 1, and 10, respectively.

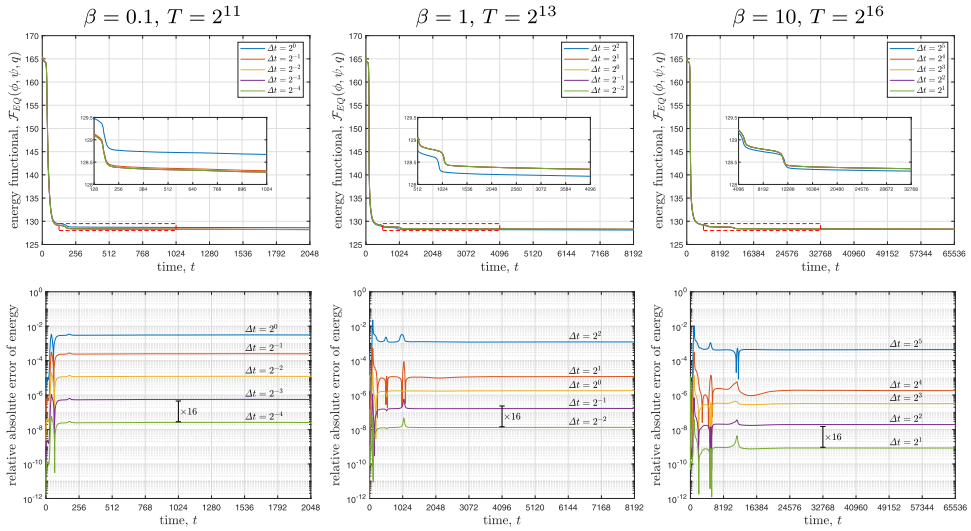

Figure 8. Evolution and relative error of the energy functional.

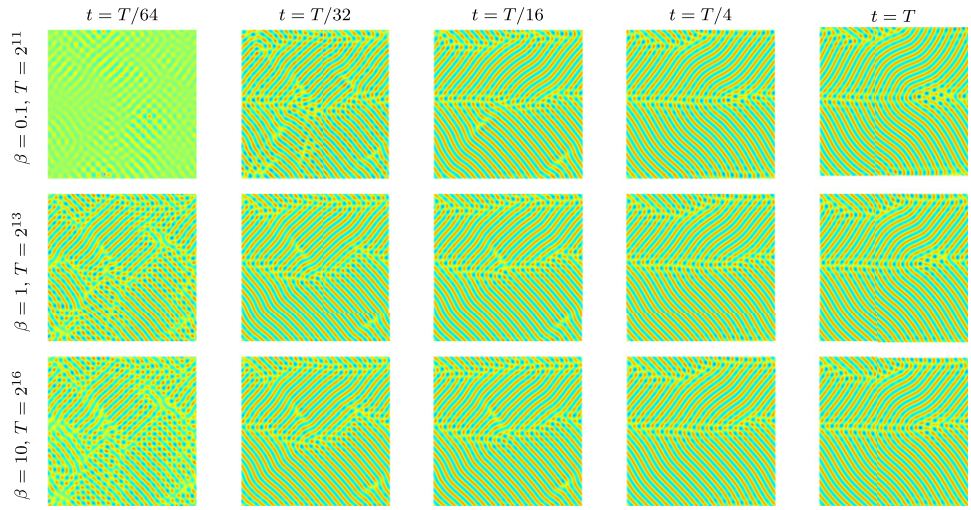

Figure 9. Solution evolutions for each β with the corresponding final time T.

Figure 9 shows the time evolution of the solution where the red, green, and blue regions indicate $\phi = 1$, 0, and -1, respectively. For each simulation, we set the same initial conditions, as shown in figure 7, and evolve this model with a sufficiently well-resolved time step, $\Delta t = 2^{-1}$, 2, and 2^4 for $\beta = 0.1$, 1, and 10, respectively. The solutions at the scaled times in figure 9 are quite similar despite the differences in the energy evolution patterns in figure 8. We numerically conclude that the steady-state solution under the same initial conditions is independent from parameter β.

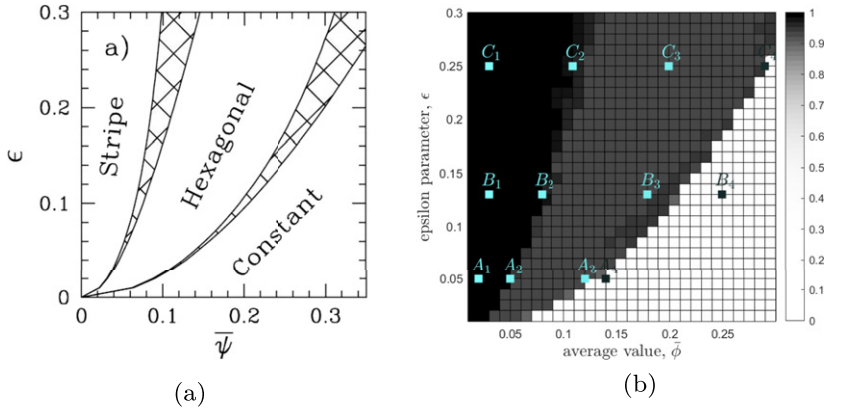

(a) (b)

Figure 10. (a) Phase diagram (reprinted with permission from [3]) and (b) values of the indicator function $\Lambda(\phi(\cdot, T))$ for the PFC equation (reprinted with permission from [14]). Here, $\bar{\psi}$ is the average value, which is identical to $\bar{\phi}$.

3.3. Pattern formation depending on various $\bar{\phi}$ and ϵ

To characterize the formation of the solutions as striped, hexagonal, or homogeneous patterns, we use the indicator function of the solution ϕ in [14]

$$\Lambda(\phi) = \frac{\int_\Omega \left|\phi - \bar{\phi}\right| \mathrm{d}\mathbf{x}}{\int_\Omega \left|\nabla\left(\phi - \bar{\phi}\right)\right| \mathrm{d}\mathbf{x}}. \tag{43}$$

Figure 10(a) shows a phase diagram described in [3] based on the linearized theory, and figure 10(b) shows the checkerboard plot for $\Lambda(\phi)$ described in [14] by solving the PFC equation. The value of the indicator function (43) can distinguish the different regions of the phase diagram.

To compare the values of the indicator function with the different parameters of β, we also employ the fourth-order method and evolve the MPFC equation for $\Omega = [0, 128] \times [0, 128]$. For the numerical simulation, we set the randomly perturbed initial condition

$$\begin{aligned}
&\phi(x, y, 0) = \bar{\phi} + 0.005 \sum_{l=0}^{8} \sum_{m=0}^{8} \mathrm{Re}\left[a_{lm} e^{\frac{2\pi i l x}{128}}\right] \cdot \mathrm{Re}\left[b_{lm} e^{\frac{2\pi i m y}{128}}\right], \\
&\psi(x, y, 0) = 0, \\
&q(x, y, 0) = \sqrt{F(\phi(x, y, 0)) + C_0},
\end{aligned} \tag{44}$$

where a_{lm} and b_{lm} are random complex numbers with $\|a_{lm}\|_\infty \leqslant 1$ and $\|b_{lm}\|_\infty \leqslant 1$. We employ (44) for the initial conditions, $\Delta x = \Delta y = 1/2$ for the grid sizes, and $\Delta t = 2^{-1}$, 2, and 2^4 for $\beta = 0.1$, 1, and 10, respectively.

Figure 11 shows the value of the indicator function $\Lambda(\phi)$ for selected parameters of $\epsilon = 0.05$, 0.13, and 0.25 with respect to the varying $\bar{\phi}$ with increments of 0.01 (we add a small constant 10^{-10} to the denominator of the indicator function to avoid dividing by zero when the pattern indicates a near constant). We observe that the indicator function value for the steady-state solution is independent of the value of β for the given parameters $\bar{\phi}$ and ϵ. To confirm the observation, we set $\epsilon = 0.13$ and present the numerical solutions at the corresponding final

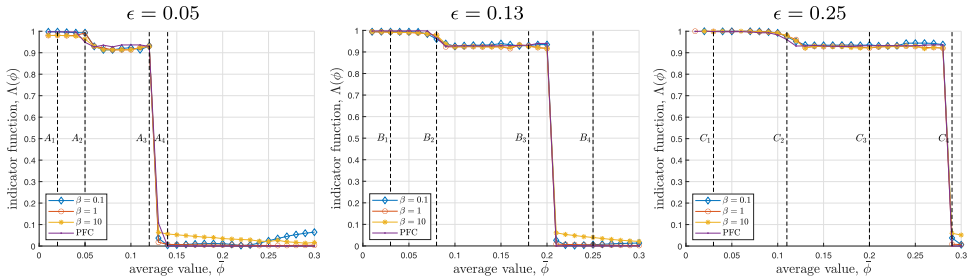

Figure 11. Values of indicator function $\Lambda(\phi)$ for several values of epsilon, i.e. $\epsilon = 0.05, 0.13, 0.25$.

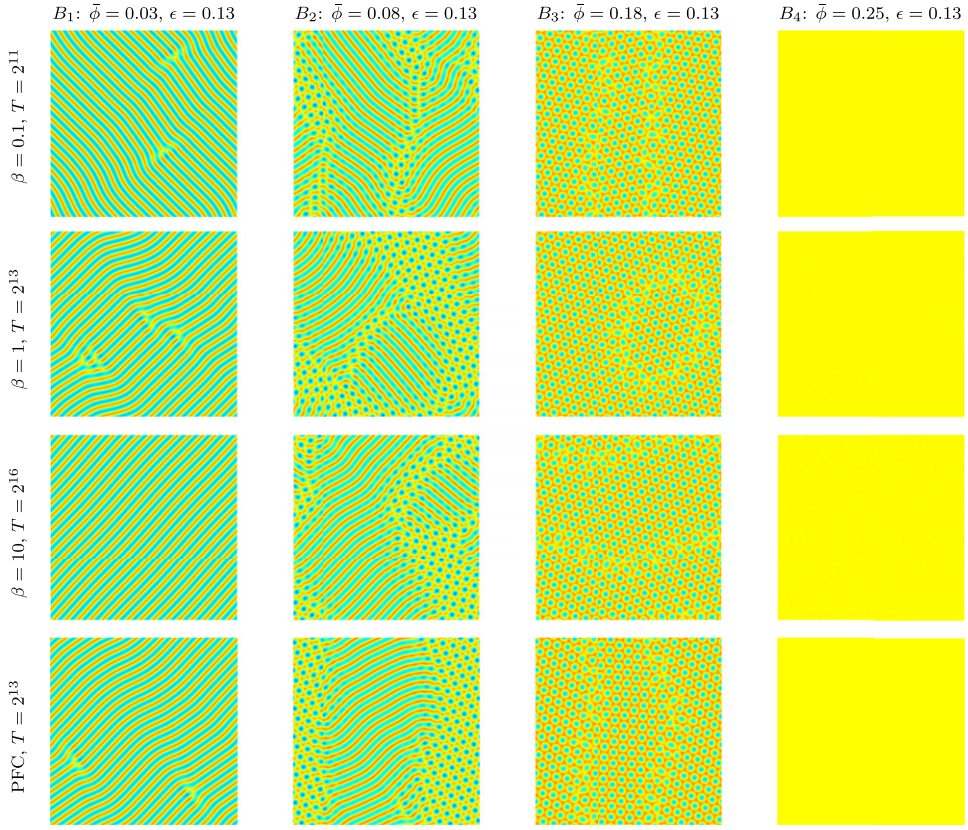

Figure 12. Solutions $\phi(x, y, T)$ of the MPFC equation with various parameters $\bar{\phi}$ and β in the case of $\epsilon = 0.13$. The last row is for the PFC equation (reprinted with permission from [14]).

times for several $\beta = 0.1$, 1, 10 in figure 12. The specific parameters $\bar{\phi}$ are for the case of B_i, as indicated in figure 10(b). For comparison, we add the results for the PFC equation in the fourth row. For each column, we can observe the stripe, coexistence, hexagon, and constant patterns regardless of the value of β.

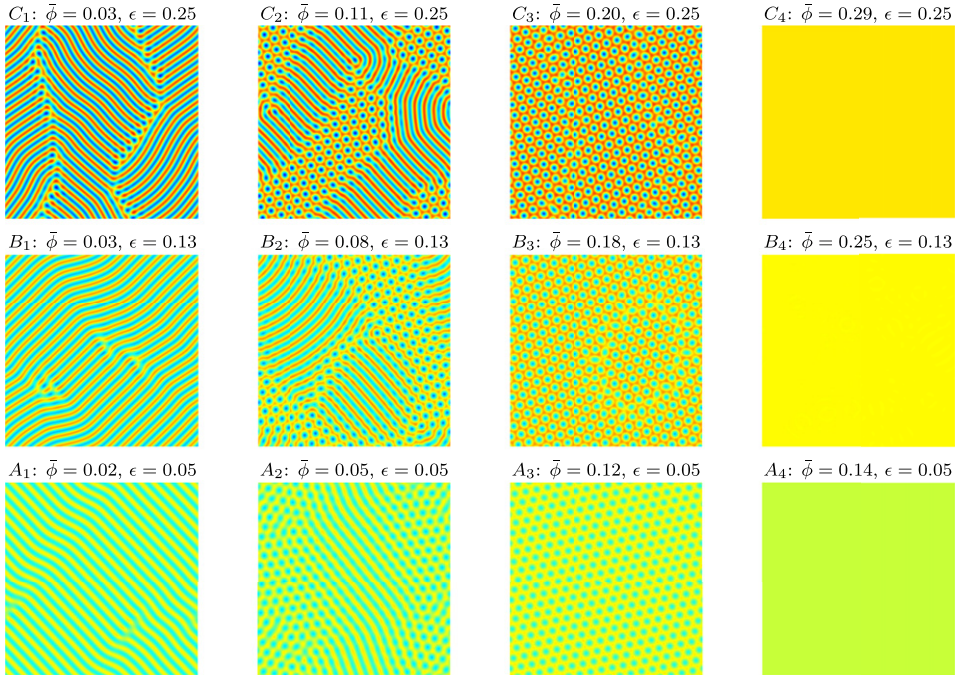

Figure 13. Long-term solutions with various $\bar{\phi}$ and ϵ in the case of $\beta = 1$.

The pattern formation of the MPFC equation seems not to depend on the β parameter, particularly close to a steady state. For a comparison with the results of the PFC equation, we choose $\beta = 1$ and evolve the solution up to $T = 2^{13}$ with various parameters of $\bar{\phi}$ and ϵ. Figure 13 shows the numerical solutions at the final time. The specific parameters $\bar{\phi}$ and ϵ are written above each figure and are indicated in figure 10(b). To compare the magnitude of the solutions, we assign colors as indicator levels, making regions in red, green, and blue to denote $\phi = 1$, 0, and -1, respectively. In general, as the parameter ϵ increases, the magnitude of the solutions increases from the bottom to the top row. By contrast, the formation of patterns consisting of stripes, which evolve into hexagons, and finally into a constant pattern, is clearly demonstrated when observing the columns from left to right. Furthermore, the snapshots in the second column show the coexistence of striped and hexagonal patterns. We numerically confirm that the pattern formation of the MPFC equation for the given $\bar{\phi}$ and ϵ is independent of β and is quite similar to the result of the PFC equation in [14].

4. Conclusions

In this paper, we proposed high order methods that guarantee the energy dissipation property to solve the MPFC equation by considering the EQRK method. Hence, we have provided detailed proofs of the mass conservation and the unconditional energy stability of the proposed method. The results of various numerical experiments have demonstrated that energy stability is attained with the desired time accuracy. Employing an indicator function to characterize the pattern formation, we compared long-term simulations with respect to the β parameter. As a result, we can infer that the patterns in the long-term evolution do not depend on β and are comparable with the results for the PFC equation.

Acknowledgments

This research was supported by the Basic Science Research Program through the National Research Foundation of Korea (NRF), funded by the Korean Government MSIP (2019R1A6A1A1-1051177, 2019R1C1C1-011112, 2020R1C1C1A0-1013468).

Data availability statement

All data that support the findings of this study are included within the article (and any supplementary files).

ORCID iDs

Jaemin Shin https://orcid.org/0000-0002-5065-4358
Hyun Geun Lee https://orcid.org/0000-0001-5135-195X
June-Yub Lee https://orcid.org/0000-0001-8029-4931

References

[1] Stefanovic P, Haataja M and Provatas N 2006 *Phys. Rev. Lett.* **96** 225504
[2] Stefanovic P, Haataja M and Provatas N 2009 *Phys. Rev.* E **80** 046107
[3] Elder K R, Katakowski M, Haataja M and Grant M 2002 *Phys. Rev. Lett.* **88** 245701
[4] Elder K and Grant M 2004 *Phys. Rev.* E **70** 051605
[5] Hu Z, Wise S M, Wang C and Lowengrub J S 2009 *J. Comput. Phys.* **228** 5323–39
[6] Shen J, Yang X and Yang X 2010 *Discrete Contin. Dyn. Syst.* **28** 1669
[7] Gomez H and Hughes T J R 2011 *J. Comput. Phys.* **230** 5310–27
[8] Shin J, Lee H G and Lee J-Y 2017 *J. Comput. Phys.* **347** 367–81
[9] Shen J, Xu J and Yang J 2018 *J. Comput. Phys.* **353** 407–16
[10] Gong Y and Zhao J 2019 *Appl. Math. Lett.* **94** 224–31
[11] Bui T Q *et al* 2020 *Modelling Simul. Mater. Sci. Eng.* **28** 025005
[12] Vignal P, Dalcin L, Brown D L, Collier N and Calo V M 2015 *Comput. Struct.* **158** 355–68
[13] Shin J, Lee H G and Lee J-Y 2016 *J. Comput. Phys.* **327** 519–42
[14] Shin J, Lee H G and Lee J-Y 2020 *Comput. Methods Appl. Mech. Eng.* **364** 112981
[15] Zhang Z, Ma Y and Qiao Z 2013 *J. Comput. Phys.* **249** 204–15
[16] Gomez H and Nogueira X 2012 *Comput. Methods Appl. Mech. Eng.* **249–252** 52–61
[17] Yang X and Han D 2017 *J. Comput. Phys.* **330** 1116–34
[18] Baskaran A, Lowengrub J S, Wang C and Wise S M 2013 *SIAM J. Numer. Anal.* **51** 2851–73
[19] Lee H G, Shin J and Lee J-Y 2017 *Comput. Methods Appl. Mech. Eng.* **321** 1–17
[20] Guo R and Xu Y 2018 *Commun. Comput. Phys.* **24** 123–51
[21] Galenko P, Gomez H, Kropotin N and Elder K 2013 *Phys. Rev.* E **88** 013310
[22] Yang X 2016 *J. Comput. Phys.* **327** 294–316
[23] Li Q, Mei L, Yang X and Li Y 2019 *Adv. Comput. Math.* **45** 1551–80
[24] Liu Z and Chen S 2021 *Appl. Numer. Math.* **163** 1–14
[25] Wanner G and Hairer E 1996 *Solving Ordinary Differential Equations II* vol 375 (Berlin: Springer)
[26] Hairer E, Hochbruck M, Iserles A and Lubich C 2006 *Oberwolfach Rep.* **3** 805–82